Distinguishing Individual Lipid Headgroup Mobility and Phase Transitions in Raft-Forming Lipid Mixtures with ^{31}P MAS NMR

Gregory P. Holland, Sarah K. McIntyre, and Todd M. Alam
Department of Electronic and Nanostructured Materials, Sandia National Laboratories, Albuquerque, New Mexico 87185-0886

ABSTRACT A model membrane system composed of egg sphingomyelin (SM), 1,2-dioleoyl-*sn*-glycero-3-phosphocholine (DOPC), and cholesterol was studied with static and magic angle spinning ^{31}P NMR spectroscopy. This model membrane system is of significant biological relevance since it is known to form lipid rafts. ^{31}P NMR under magic angle spinning conditions resolves the SM and DOPC headgroup resonances allowing for extraction of the ^{31}P NMR parameters for the individual lipid components. The isotropic chemical shift, chemical shift anisotropy, and asymmetry parameter can be extracted from the spinning side band manifold of the individual components that form liquid-ordered and liquid-disordered domains. The magnitude of the ^{31}P chemical shift anisotropy and the line width is used to determine headgroup mobility and monitor the gel-to-gel and gel-to-liquid crystalline phase transitions of SM as a function of temperature in these mixtures. Spin-spin relaxation measurements are in agreement with the line width results, reflecting mobility differences and some heterogeneities. It will be shown that the presence of DOPC and/or cholesterol greatly impacts the headgroup mobility of SM both above and below the liquid crystalline phase transition temperature, whereas DOPC displays only minor variations in these lipid mixtures.

INTRODUCTION

The formation and detection of lipid rafts in biomembranes have attracted much attention in recent years due to their potential role in signal transduction, cholesterol shuttling, and protein sorting (1–6). Lipid rafts are thought to be involved in the trafficking and formation of proteins associated with prion and Alzheimer's diseases (7,8), and as potential sites for toxin interactions and entryways for pathogens (9). For example, it has become widely accepted that lipid rafts play a key role in how HIV-1 fuses to cell membranes (10–12). Although their biological relevance and importance are apparent, the way in which lipid rafts self assemble and organize on a molecular to nanometer scale is still far from understood.

Lipid rafts are liquid-ordered domains (l_o) rich in saturated lipids and cholesterol floating in a sea of liquid-disordered (l_d) phospholipids that are cholesterol-poor. The first evidence for the existence of lipid rafts was the detection of detergent-resistant membranes that were insoluble in Triton X-100 (13). These insoluble phases were composed primarily of sphingolipids and cholesterol. The raft phase is believed to be in a l_o state, whereas the more fluid phase has a high content of unsaturated phospholipids and exists in the l_d state. Although there have been various lipid raft systems studied, the two most common models appear to be the 1,2-dioleoyl-*sn*-glycero-3-phosphocholine/1,2-dipalmitoyl-*sn*-glycero-3-phosphocholine/cholesterol (DOPC/DPPC/Chol) and 1,2-dioleoyl-*sn*-glycero-3-phosphocholine/sphingomyelin/cholesterol (DOPC/SM/Chol) systems. Raft formation has been observed experimentally in both of these model membrane systems with various techniques, including fluorescence microscopy (14–19), ^{2}H NMR (17), pulsed field gradient (PFG) NMR (20), electron spin resonance (21), atomic force microscopy (22,23), x-ray diffraction (24), and neutron scattering (25). Phase diagrams have been constructed for both DPPC (18) and SM (14,26) ternary systems containing DOPC and Chol. Some of these phase diagrams have led to a thermodynamic model involving condensed complexes (27). In these systems, DPPC or SM forms the raft phase by incorporating Chol that preferentially packs with the saturated chains, whereas the unsaturated chains of DOPC comprise the ''disordered sea'' in which the lipid rafts are dispersed.

Static ^{31}P NMR has been extensively used for decades to study the structure and dynamics of multilamellar vesicles in various phospholipid systems (28–30). These static NMR experiments produce ^{31}P powder patterns that result solely from the chemical shift anisotropy (CSA) when ^{1}H decoupling is applied. The ^{31}P CSA is sensitive to both headgroup geometry and local dynamics. The phospholipid headgroup conformation can be extracted from the ^{31}P CSA by orienting the membrane with respect to the NMR external magnetic field (31). Since the CSA interaction is also sensitive to the headgroup dynamics, it has been successfully implemented to determine the types of local motions occurring in the gel (L_β), intermediate ($P_{\beta'}$), and liquid crystalline phases (L_α) of phospholipid membranes (32–34). The presence of cholesterol (35,36) and the degree of hydration (37) can greatly impact the CSA and provide insight into the interaction between the phospholipid and other select constituents.

Static ^{31}P NMR has been used to study a limited number of raft-forming mixtures (38–41). This method often suffers

Submitted November 7, 2005, and accepted for publication February 22, 2006.

Address reprint requests to Todd M. Alam, E-mail: tmalam@sandia.gov.

© 2006 by the Biophysical Society

0006-3495/06/06/4248/13 $2.00

doi: 10.1529/biophysj.105.077289

due to a lack of resolution resulting from overlapping powder patterns that make determination of the ^{31}P CSA of the individual lipid components difficult (40,41). In contrast, ^{31}P magic angle spinning (MAS) NMR resolves resonances from distinct headgroup environments and is being implemented to a greater extent in the study of multi-component lipid mixtures (42–49). Another advantage of MAS NMR is that it requires significantly less sample compared to static NMR methods. In this work, we chose to study the mixture of DOPC/SM/Chol since the ^{31}P NMR isotropic chemical shifts of the SM and DOPC headgroups are resolvable under moderate MAS conditions. This permits extraction of the ^{31}P CSA parameters (from the spinning sideband manifold), line widths, and relaxation times of the individual lipid components that form the l_o and l_d domains.

MATERIALS AND METHODS

Materials

Egg SM, DOPC, and Chol were obtained from Avanti Polar Lipids (Alabaster, AL) and used as received. The SM had the following acyl chain composition: 84% 16:0, 6% 18:0, 2% 20:0, 4% 22:0, and 4% 24:0, and contained no unsaturated acyl chains.

Sample preparation

Pure lipid samples were prepared by mixing the lipid with deionized water (pH = 7.5) in a conical vial with a vortex mixer. This was followed by a minimum of five freeze-thaw cycles in dry ice and a warm water bath set to 333 K (above the liquid crystalline phase transition for DOPC and SM). Buffer was not used in any of the lipid mixtures to prevent multilamellar vesicle (MLV) fragmentation due to freeze-thaw cycling in the presence of salt (50). Thus, the samples in this study are large MLVs $>\sim 1$ μm in diameter. Samples containing multiple lipid constituents were first combined and dissolved in chloroform followed by vacuum drying overnight to remove the solvent. The samples were then hydrated with the above procedure. All lipid samples were 33 wt % phospholipid. The binary Chol-containing samples were 33 mol % Chol to be consistent with the Chol content of the raft-forming lipid mixture that was 1:1:1 mol %. The lipid samples were transferred to 4 mm zirconia MAS rotors and sealed with kel-F inserts and caps. The typical volume of MLV samples for NMR analysis was 50–100 μL, corresponding to 25–50 mg of phospholipid. The samples were stored in a −20°C freezer when NMR experiments were not being performed.

^{31}P NMR spectroscopy

^{31}P NMR spectra were collected on a Bruker (Karlsruhe, Germany) Avance 600 spectrometer equipped with a 4 mm broad band MAS probe under both static and MAS conditions. The MAS speed was set to 2 kHz and controlled to ±1 Hz in all MAS experiments. The temperature was varied between 296 and 320 K and controlled to ±0.2 K with a Bruker variable temperature unit. Static spectra were obtained with a spin-echo sequence ($\pi/2 - \tau - \pi$), where the $\pi/2$ pulse was 4.5 μs and the interpulse delay, τ, was 20 μs. A moderate ^{1}H two pulse phase modulation decoupling field strength of 22.5 kHz was applied after the $\pi/2$ pulse through acquisition of the free induction decay using a 15° phase shift (51). For the MAS experiments, a single pulse Bloch decay without ^{1}H decoupling was utilized. Spin-spin relaxation measurements (T_2) were performed under MAS conditions with a rotor synchronized spin-echo. A recycle delay of 3 s was utilized in all experiments. The isotropic chemical shift was set using the secondary reference of solid $NH_4H_2PO_4$ ($\delta = +0.8$ ppm with respect to phosphoric acid $\delta = 0$ ppm). The extraction of the ^{31}P CSA ($\Delta\sigma$), asymmetry parameter (η), full width at half-maximum (FWHM), and deconvolutions necessary for T_2 fitting were performed with the DMFIT software package (52). The uncertainty in the FWHM ranged from ±2 to ±5 Hz, whereas the uncertainty in the determined $\Delta\sigma$ is ± 0.2 ppm.

Due to the phosphorous headgroup rotational motion about the lipid bilayer normal in MLVs, the chemical shielding tensor is averaged to an effective tensor that is axially symmetric. The anisotropic part of this time-averaged tensor has been defined by Seelig as

$$\Delta\sigma = \sigma_{\parallel} - \sigma_{\perp} = \frac{3}{2}(\sigma_{\parallel} - \sigma_{\mathrm{i}}), \tag{1}$$

where σ_{i} is the isotropic chemical shift, $\sigma_{\parallel}$ is the low intensity shoulder ($\sigma_{\parallel} = \sigma_{33}$), and $\sigma_{\perp}$ is the high intensity shoulder ($\sigma_{\perp} = \sigma_{11} = \sigma_{22}$) of the axially symmetric powder pattern (29). This definition of $\Delta\sigma$ differs from the formalism used in the DMFIT software package by a factor of 3/2 where the anisotropy from DMFIT ($\Delta\delta$) is given by

$$\Delta\delta = \sigma_{33} - \sigma_{\mathrm{i}} \tag{2}$$

and has been accounted for in the $\Delta\sigma$ reported here to remain consistent with the earlier ^{31}P work on phospholipid membranes (28,29,31,35,37). The asymmetry parameter of the ^{31}P shielding tensor is defined as

$$\eta = \frac{(\sigma_{22} - \sigma_{11})}{(\sigma_{33} - \sigma_{\mathrm{i}})}, \tag{3}$$

where the principal components of the tensor are ordered in the following manner: $|\sigma_{33} - \sigma_{\mathrm{i}}| > |\sigma_{22} - \sigma_{\mathrm{i}}| > |\sigma_{11} - \sigma_{\mathrm{i}}|$. In the DMFIT program, the minimization of the fitting error uses a quadratic distance between the simulated and experimental spectra with an iterative constrained gradient protocol involving the partial derivatives of all parameters in the line shape model (52). For chemically shifted resolved components, the fits for both the static and MAS spectra were relatively sensitive to variations in $\Delta\sigma$, η, and the line-width. The exception to this was the situation where an overlap of two different SM line shapes were present, in which case the fits of the MAS NMR spectra were poorly behaved. For these overlapping MAS simulations the value of η was fixed to that obtained from the static spectra to improve convergence.

RESULTS AND DISCUSSION

Static ^{31}P NMR characterization

The static ^{31}P NMR spectra for SM, SM/Chol, DOPC, DOPC/Chol, DOPC/SM, and DOPC/SM/Chol are displayed in Fig. 1 at two different temperatures. In all these mixtures, DOPC is above its liquid crystalline phase transition temperature (T_m) of 255.7 K, and should exist in the L_α liquid crystalline state (53). SM has a T_m of ~313 K and therefore is in either the gel or liquid crystalline state, depending on the observation temperature, 296 K or 318 K, respectively (54,55). For SM in the gel phase (Fig. 1 *A*, 296 K), the ^{31}P powder pattern is composed of two components: one that is axially asymmetric with $\Delta\sigma = 56.1$ ppm and $\eta = 0.7$, and an axially symmetric pattern with $\Delta\sigma = 54.0$ ppm and $\eta = 0.0$. This result is consistent with previous static ^{31}P NMR results on SM in the gel phase where both an axially symmetric component and an asymmetric component were required to fit the ^{31}P powder pattern (56). When the temperature is

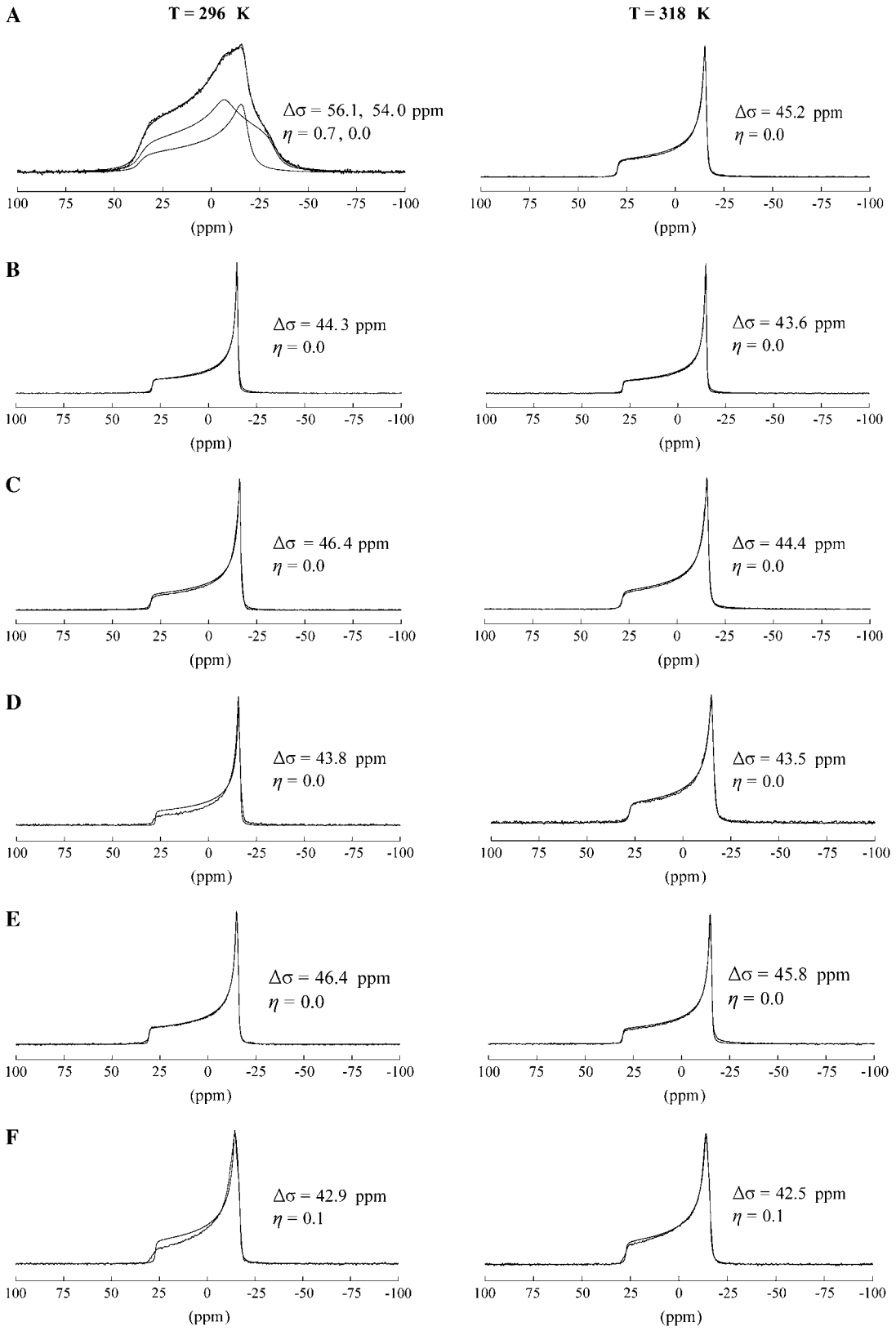

FIGURE 1 Static ^{31}P NMR spectra of (*A*) SM, (*B*) SM/Chol (33 mol%), (*C*) DOPC, (*D*) DOPC/Chol (33 mol%), (*E*) DOPC/SM, and (*F*) DOPC/SM/Chol. Spectra collected at temperatures below (296 K) and above (318 K) the T_m (~313 K) of SM are shown. The fits with the extracted CSA parameters are also displayed in the figure.

raised above the L_α phase transition (Fig. 1 *A*, 318 K), the static ^{31}P NMR spectrum of SM collapses to a single, axially symmetric component ($\eta = 0$) with $\Delta\sigma = 45.2$ ppm. This $\Delta\sigma$ is slightly larger than that recently reported for oriented egg SM (34) and close to the value of 45.8 ppm reported by Shaikh et al. on unoriented SM (38). This dynamically averaged ^{31}P powder pattern results from axial rotation of the phosphodiester moiety about the bilayer normal, bond librations, and overall lipid fluctuations and rotations (33,57). The substantially smaller CSA of the L_α state compared to the L_β state is attributed to the considerable decrease in the correlation times of these headgroup motions by greater than one to two orders of magnitude (33).

The binary SM/Chol sample (Fig. 1 *B*) displays an axially symmetric powder pattern ($\eta = 0$) both above and below the L_α phase transition (~313 K), with a $\Delta\sigma \sim 44$ ppm. This axially symmetric CSA is similar to pure SM in the L_α state, but the presence of Chol has reduced $\Delta\sigma$ by ~3%. Similar results were observed for bovine brain SM bilayers containing cholesterol, where an axially symmetric powder pattern was observed below the L_α phase transition of SM down to 0°C (36). This reduction in $\Delta\sigma$ at 296 K (below T_m) presumably occurs due to a partitioning of cholesterol between the SM lipid molecules in the bilayer that disrupts the packing of the saturated chains and permits headgroup rotation similar to that occurring in the L_α phase of pure SM. The effect of Chol incorporation on phospholipid bilayers has been previously monitored with static ^{2}H and ^{31}P NMR, where the dynamic averaging of the hydrocarbon chain and headgroup regions of the lipid was monitored with the two techniques, respectively (35). ^{2}H NMR detected an increase in the ordering of the hydrocarbon chain above T_m with the incorporation of Chol, whereas ^{31}P NMR revealed a decrease in the ordering of the headgroup moiety below T_m when Chol is incorporated in the bilayer.

The DOPC (Fig. 1 *C*) and DOPC/Chol (Fig. 1 *D*) samples yield similar axially symmetric ($\eta = 0$) powder patterns at both temperatures since both are above the T_m of DOPC (255.7 K). The Chol-containing sample reveals a CSA ~2 ppm smaller at 296 K and ~1 ppm smaller at 318 K compared to pure DOPC. This change in ^{31}P CSA is consistent with previous studies on DOPC bilayers containing cholesterol where an ~2 ppm decrease in CSA was also observed (58). This result shows that although small, Chol has a detectable effect on the ^{31}P CSA of DOPC in the L_α state. Similar observations have been reported for the ^{31}P CSA of DPPC and 1,2-dipalmitoyl-*sn*-glycero-3-phosphoethanolamine in the L_α phase, where an ~2–3 ppm decrease was observed for 1:1 mixtures with cholesterol (35,59). This small decrease in headgroup ordering in DOPC with incorporation of Chol occurs in conjunction with an increased degree of chain ordering as revealed by ^{2}H NMR (22).

The binary DOPC/SM mixture (Fig. 1 *E*) exhibits a single axially symmetric pattern with a CSA comparable to the pure DOPC sample or the SM/Chol mixture. There is no evidence of overlapping powder patterns as seen in the pure SM (Fig. 1 *A*) sample. This result shows that DOPC has a similar influence on the dynamics of the headgroup region of SM as cholesterol does; increasing the headgroup dynamics that occur below T_m. This experimental observation provides strong evidence that SM and DOPC are completely miscible in this mixture, displaying no sign of phase separation.

The ternary raft-forming phase DOPC/SM/Chol (Fig. 1 *F*) results in a slightly asymmetric powder pattern with $\Delta\sigma =$ ~43 ppm and $\eta = 0.1$ above and below the L_α phase transition of SM.

The asymmetric shape ($\eta \neq 0$) of the raft-forming mixture DOPC/SM/Chol could provide some evidence for overlapping axially symmetric CSA powder patterns. Previous static ^{31}P NMR on related POPE/SM/Chol mixtures gave results that were similar, although much clearer shoulders were observed in that study permitting the extraction of the individual CSA parameters for POPE and SM from spectral simulation of the static ^{31}P NMR line shape (38). Although DOPC and SM have indistinguishable CSA powder patterns in the ternary phase (Fig. 1 *F*), the isotropic chemical shift can be resolved under one-dimensional MAS conditions, and was pursued to extract the ^{31}P CSA parameters of the individual components (discussed in the next section).

In a previous static ^{31}P NMR study on DOPC/SM/Chol, a splitting of the powder pattern was observed that was attributed to potential phase separation as the Chol content was increased to a value of 30 mol % (39). This splitting of the ^{31}P powder pattern was not observed here; however, the asymmetric shape could indicate the presence of two overlapping patterns. It is also important to note that no isotropic components ($\delta \sim 0$) were observed in any of the static ^{31}P NMR spectra shown in Fig. 1. This indicates that stable bilayers (> 500 nm) were formed in all of these samples with no spherical micelle structures or regions of high bilayer curvature leading to isotropic averaging of the ^{31}P CSA tensor.

^{31}P MAS NMR characterization of binary systems

The ^{31}P MAS NMR spectra were also collected on the six lipid mixtures and are presented in Fig. 2. The spinning sideband manifold for pure SM was fit with a symmetric ($\Delta\sigma = 49.4$ ppm, $\eta = 0.0$) and an asymmetric ($\Delta\sigma = 56.8$ ppm, $\eta = 0.7$) component to maintain consistency with the static model below T_m (Fig. 2 *A*, 296 K). The line widths (FWHM = 700, 250 Hz) are broad compared to the MAS spectra of the other lipid mixtures and the two components extracted from the static ^{31}P NMR spectrum are not as apparent. As noted in the Materials and Methods section, these overlapping MAS simulations are poorly constrained and required fixing of the η-values from those obtained from the static NMR spectra. It is also possible to fit the pure SM (below T_m) with a single spectra component, but the error was slightly larger than that obtained with the overlapping two

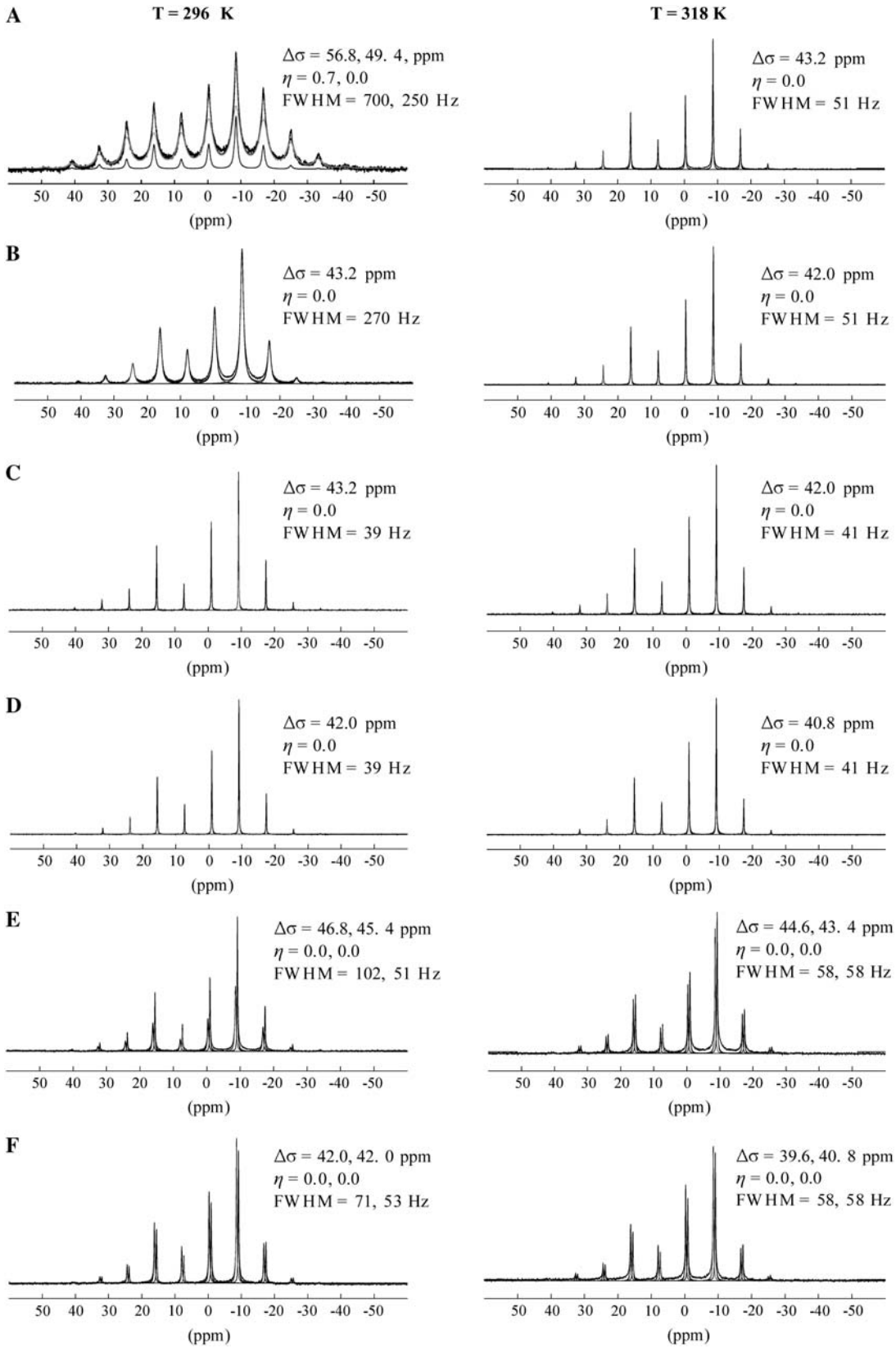

FIGURE 2 ^{31}P MAS NMR spectra of (*A*) SM, (*B*) SM/Chol (33 mol%), (*C*) DOPC, (*D*) DOPC/Chol (33 mol%), (*E*) DOPC/SM, and (*F*) DOPC/SM/Chol. Spectra collected at temperatures below (296 K) and above (318 K) the T_m of SM are shown. The fits with the extracted CSA parameters are also displayed in the figure. The parameters extracted for SM are indicated first for samples containing both SM and DOPC.

component simulation. This result shows an example in which it can often be advantageous to run both static and MAS NMR to detect multiple phases in heterogeneous lipids like SM. Above T_m (Fig. 2 *A*, 318 K), the ^{31}P MAS NMR spectrum shows an axially symmetric powder pattern with a dramatically decreased CSA ($\Delta\sigma$ = 43.2 ppm) and line width (FWHM = 51 Hz) compared to the gel phase. This is in agreement with the static observations of unoriented and oriented samples and consistent with SM being in the L_α state (34).

The ^{31}P MAS spectrum of the SM/Chol sample (Fig. 2 *B*, 296 K) displayed a significant decrease in $\Delta\sigma$ compared to the pure SM sample below T_m (Fig. 2 *A*, 296 K) similar to the static results. For this mixture, the MAS line width (FWHM = 270 Hz) is much broader than the line width (FWHM = 51 Hz) for the pure SM sample in the L_α phase (Fig. 2 *A*, 318 K). This shows that although the magnitude of the CSA decreases for the SM/Chol mixture (below T_m) to a value comparable to that observed in the pure SM L_α state, the SM headgroup dynamics in the Chol-containing sample are not identical to the L_α phase of pure SM. Above T_m, the SM/Chol sample does display a line width (FWHM = 51 Hz) comparable to the L_α phase of pure SM. This change in line width when the temperature is increased from 296 K to 318 K provides strong evidence that the SM/Chol sample does undergo some form of phase transition involving a decrease in molecular correlation times that is more easily discernable as a change in the MAS line width than a change in ^{31}P CSA (discussed further below).

The ^{31}P MAS NMR spectra of the DOPC (Fig. 2 *C*) and DOPC/Chol (Fig. 2 *D*) samples display very similar behavior compared to the static spectra at 296 K and 318 K. Axially symmetric spinning sideband patterns are observed with slightly smaller CSAs (~1 ppm) for the Chol-containing samples at both temperatures. The line widths are very similar for measurements made on both samples at both temperatures (FWHM $\approx$ 40 Hz). This is consistent with DOPC being in the L_α phase in all four experiments. It should be noted that for measurements on SM and DOPC in the presence of Chol and without, the magnitude of the CSA extracted from the MAS spectra are slightly smaller than those observed under static conditions. The reason static spectra yield slightly larger CSAs compared to the MAS spectra is not clear; however, one possibility for the discrepancy could be due to partial alignment of the lipid bilayers in the high NMR magnetic field. Lipid molecules have a negative anisotropic magnetic susceptibility, and thus have a tendency to align with their long axis perpendicular to the magnetic field. This results in the MLV having an ellipsoidal shape that skews the resulting ^{31}P powder pattern (60). The fits of the static ^{31}P spectra obtained in this study assume a random distribution of orientations. This assumption could be a possible source of error. Under MAS conditions, the orientational ordering is dramatically reduced (61). Therefore, the CSAs extracted from MAS spectra are presumably more accurate than the ones extracted from the static spectra. Further, it has been theoretically shown that MAS spectra give more reliable results than static spectra when extracting the magnitude of the CSA (62). When comparing static-to-static spectra and MAS-to-MAS spectra, the variations observed for the different samples are consistent.

^{31}P MAS NMR characterization of ternary mixtures

The ^{31}P MAS NMR spectra for the DOPC/SM and DOPC/SM/Chol samples are shown in Fig. 2, *E* and *F*, respectively. The ^{31}P MAS NMR spectrum of the DOPC/SM sample resolves the isotropic chemical shift of DOPC and SM that are −1.0 and −0.4 ppm. In contrast to the glycerol backbone in DOPC, the SM lipid possesses a sphingosine backbone allowing for intermolecular hydrogen bonding between the C3 hydroxyl group and the amide hydrogen, plus intramolecular hydrogen bonding between the hydroxyl group and the phosphoryl oxygen of the headgroup. Molecular dynamics simulations (63,64) and ^{31}P liquid-state NMR (65) results favor the later intramolecular hydrogen bonding pair, although a finite possibility also exists for intramolecular hydrogen bonding between the phosphoryl oxygen and the amide hydrogen, according to one of the molecular dynamics studies (64). This 0.6 ppm decrease in the ^{31}P chemical shift in comparing DOPC and SM has been attributed to the presence of these hydrogen bonding motifs within SM that do not exist in phosphatidylcholines (66). The presence of these different hydrogen bonding arrangements may result in differences in the headgroup interaction with water between the two lipids. An expansion of the isotropic chemical shift range is shown in Fig. 3, where the resonance lines of the pure components can be compared with the mixtures. The isotropic ^{31}P chemical shifts for the individual lipid headgroups in the DOPC/SM mixture were identical to the pure lipid chemical shifts and did not vary as a function of temperature or with addition of cholesterol (33 mol %), arguing that if hydrogen bonding is responsible for the decrease in the ^{31}P chemical shift of SM, the hydrogen bonding motif does not appear to vary for the different mixtures and temperatures investigated.

Variation of ^{31}P CSA for mixtures

It is interesting to compare the magnitude of the CSA extracted from the ^{31}P MAS spectra of DOPC/SM and DOPC/SM/Chol to those of the pure lipid mixtures. In the DOPC/SM mixture at 296 K (below the T_m of SM), the CSA of DOPC is ~2 ppm larger (~5%) than the CSA observed in pure DOPC, whereas the CSA of SM is ~10 ppm smaller (~18%) than the CSA observed for pure SM (Fig. 2). For the DOPC/SM mixture, the DOPC resonance also displays ~2 ppm decrease in CSA at 318 K compared to the measurement at 296 K; however, the value of the DOPC ^{31}P CSA is ~1 ppm larger than that observed for pure DOPC at 318 K.

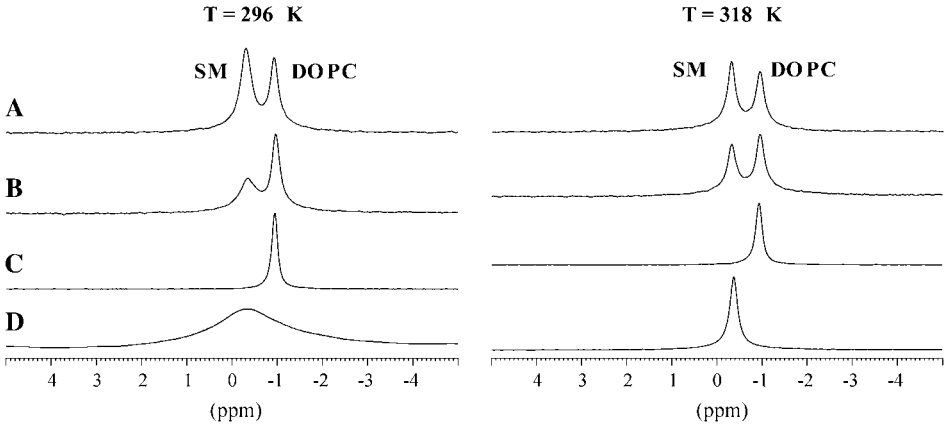

FIGURE 3 Isotropic chemical shift region of ^{31}P MAS NMR spectra of (*A*) DOPC/SM/Chol, (*B*) DOPC/SM, (*C*) DOPC, and (*D*) SM. Spectra collected below (296 K) and above (318 K) the T_m of SM are shown.

These results, along with the continued observation of the SM gel-to-L_α phase transition with temperature (see discussion below on SM ^{31}P CSA temperature variation) demonstrates that the SM is still in the ordered gel phase at 296 K. It is known that for phospholipids with different T_m that either the mixture can remain uniform or cooperative phase separation can occur, with a coexisting gel and L_α phases. If a phase separation did occur, there are limits to the lipid composition of the coexisting phases. In one limiting case, the gel phase can be assumed to be composed entirely of SM, which would predict a $\Delta\sigma \sim 55$ ppm (pure SM at 296 K), significantly larger than observed experimentally. This would also predict the L_α phase to be composed entirely of DOPC, giving rise to $\Delta\sigma \sim 42$ ppm, which is smaller than the $\Delta\sigma \sim 45.4$ ppm observed experimentally. Based on the observed headgroup dynamics, this type of pure phase separation does not appear to occur. Intermediate to this limit is a gel phase enriched in SM with a minor concentration of DOPC, along with a minor concentration of SM in the DOPC rich L_α phase. There is no evidence of two SM phases (or two DOPC phases) coexisting in the current ^{31}P NMR experiments, but it would be difficult to resolve overlapped SM (or DOPC) phases with small differences in $\Delta\sigma$. In addition, it may also be possible for the coexisting gel and L_α phases to be in rapid exchange, giving rise to an averaged $\Delta\sigma$ (see discussion below on time and length scales). To distinguish these possibilities using ^{31}P NMR will be difficult and will require careful studies of these mixtures as a function of relative concentration. For this study, we will report the single parameter or averaged $\Delta\sigma$ values assuming these lipid mixtures are homogeneous. Under this assumption, these results illustrate a cooperative effect among lipid constituents. The presence of DOPC greatly increases the SM headgroup mobility and subsequent motional averaging of the SM ^{31}P CSA tensor. These experiments also reveal that the ^{31}P CSA of DOPC does not remain unchanged with the incorporation of SM, but increases slightly, consistent with a decrease in DOPC headgroup motions, although the impact of DOPC on SM appears to be larger than the SM impact on DOPC. These observations are in agreement with the static ^{31}P experiments; however, the ^{31}P MAS NMR results are unique in that they yield an exact measure of the variation in the ^{31}P CSA for the two individual components.

A similar argument can be made for the DOPC/SM/Chol mixture where the ^{31}P CSA of SM is ~5 ppm smaller than the binary DOPC/SM sample at both 296 K and 318 K. Similarly, the ^{31}P CSA of DOPC in the DOPC/SM/Chol mixture is ~3 ppm smaller than the binary mixture. In this case, a pure phase-separated gel phase SM/Chol composition would predict a $\Delta\sigma \sim 43.2$ ppm at 296 K for SM, whereas experimentally it is ~42.0 ppm. The corresponding pure DOPC L_α would predict a $\Delta\sigma \sim 43.2$ ppm, whereas again a smaller value of 42 ppm was observed. Again in these ^{31}P MAS NMR studies, there is no evidence of this type of phase separation, but additional experiments would be required to fully unravel this. Assuming a homogeneous mixture, these experiments show that the presence of Chol increases the headgroup motion of both lipids, although the impact of Chol on the SM headgroup is larger. The fact that the SM ^{31}P CSA is smaller in the DOPC/SM/Chol mixture both above and below T_m compared to the SM/Chol (33% Chol) binary mixture could indicate a higher relative amount (>33%) of Chol present in the SM domain of the ternary mixture. However, considering the large effect DOPC has on the headgroup of SM (Fig. 2 *E*), the cooperative effect of DOPC and Chol presence cannot be ruled out as the cause of the SM ^{31}P CSA reduction in the ternary mixture. Further work is in progress where the Chol concentration is varied to distinguish these cooperative lipid effects and the sole impact of Chol, and will be presented elsewhere. These results also show that if phase separation occurs into cholesterol-rich SM domains below T_m, that there must still be some Chol present and interacting with the DOPC component, since it too displays a decrease in ^{31}P CSA to a value comparable to that observed in the DOPC/Chol binary mixture. This is in agreement with previous ^{2}H NMR and atomic force microscopy results that indicate there is cholesterol present in the DOPC l_d domains (22,23) as well as more recent PFG studies

on the DOPC/SM/Chol mixture, which show that there is preferential enrichment of Chol and SM in the l_o domains, but with lateral diffusion rates between those of pure ternary DOPC/Chol and SM/Chol mixtures (20). Again, note that the resolution of the individual headgroup resonances afforded by ^{31}P MAS NMR allows these subtle variations in the lipid headgroup dynamics to be directly measured.

Variation of ^{31}P line width for mixtures

The line widths of the ^{31}P isotropic resonances are different for the mixtures and pure lipid samples, and change as a function of temperature, particularly for SM. The ^{31}P line width of SM below its T_m is much narrower (FWHM = 102 Hz) in the mixture with DOPC (Fig. 3 *B*, 296 K) than in the pure SM sample where the FWHM = 250 and 700 Hz (Fig. 3 *D*, 296 K). However, above the T_m of SM, the ^{31}P line widths (FWHM = 58 Hz) are comparable in the DOPC/SM mixture. In the DOPC/SM/Chol sample below T_m, the line widths of the different lipid resonances are not identical, where the FWHM = 71 Hz for SM and 53 Hz for DOPC. Above T_m, comparable ^{31}P line widths are observed with the FWHM = 58 Hz for both lipid headgroups. These results show that SM undergoes a liquid crystalline phase transition, and the difference in line width between SM and DOPC below the SM T_m indicates a lower degree of mobility and/or an increased heterogeneity of headgroup environments for SM compared to DOPC. Additional discussion about this change is presented in the T_2 section below. This variation in the ^{31}P line width is consistent with prior interpretations regarding ternary mixtures of saturated lipids, unsaturated lipids, and cholesterol that form coexisting liquid phases below T_m. The saturated lipid is in a l_o state, whereas the unsaturated lipid is in a liquid crystalline l_d state (14,16,18,19). This separation into l_o and l_d phases presumably results in slight differences in mobility that are borne out in the line width. Above T_m, both DOPC and SM have comparable line widths, and therefore both appear to exist in a liquid crystalline l_d state.

Variation of the SM ^{31}P CSA with temperature

Although variations in the ^{31}P CSA have been noted above for changes in the lipid composition, it is also instructive to take a detailed look at the variation in the SM ^{31}P CSA as a function of temperature. The CSA of SM extracted from the ^{31}P MAS spectra as a function of temperature for the different lipid mixtures is displayed in Fig. 4. For pure SM, the ^{31}P CSA decreases as the temperature increases and displays two transitions: a small one at 306 K that is attributed to a gel-gel transition and a major one at 314 K that is attributed to the gel-liquid crystalline phase transition. This is in excellent agreement with previous static ^{31}P NMR results that report a gel-gel transition at 306 K and the formation of an almost exclusively L_α bilayer at 314 K for SM (56). For the pure SM, there is also a small reduction in the

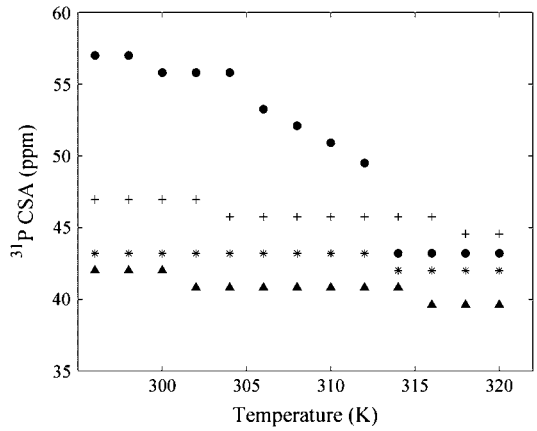

FIGURE 4 Magnitude of ^{31}P CSA ($\Delta\sigma$) extracted from fitting the MAS spinning sideband manifold for SM component as a function of temperature in lipid bilayer mixtures: (•) SM, (+) DOPC/SM, (*) SM/Chol, and (▲) DOPC/SM/Chol.

^{31}P CSA observed at 300 K, along with a gradual decrease in the CSA approaching the L_α phase transition. This gradual decrease is not surprising, considering that naturally occurring SM is heterogeneous, having different acyl chain lengths producing complex phase behavior where multiple different gel phases have been proposed (56,67), and a very broad asymmetric L_α phase transition is observed by differential scanning calorimetry (DSC) (68,69). For the other lipid mixtures (Fig. 4), changes in the ^{31}P CSA at the phase transitions are much less apparent, although some minor variations are observed. The relative decrease in the SM ^{31}P CSA occurs in the following order: SM > SM/DOPC > SM/Chol > DOPC/SM/Chol. From these trends, cholesterol has a larger impact than DOPC on the reduction of the SM ^{31}P CSA (and correspondingly the increased headgroup dynamics). Also note that DOPC and Chol have the largest combined effect on SM where the smallest ^{31}P CSA was observed for the ternary DOPC/SM/Chol mixture, again suggesting cooperative lipid effects in these mixtures. The ^{31}P CSA variations for DOPC in these mixtures as a function of temperature are very minor, reflecting that DOPC is in the L_α phase for the entire temperature range investigated.

Line width variation for SM with temperature

Since the ^{31}P MAS NMR line width (FWHM) of SM varies greatly in the different mixtures, it was also monitored as a function of temperature as shown in Fig. 5. For pure SM, the FWHM increases as the temperature is increased and the L_α phase transition is approached (~314 K). Above this transition, a drastic order of magnitude decrease in the ^{31}P FWHM is observed. The increase in ^{31}P FWHM before the L_α transition was initially surprising because the ^{31}P CSA decreases across this range, indicating an increase in motional averaging, yet a broadening of the ^{31}P resonance could be an

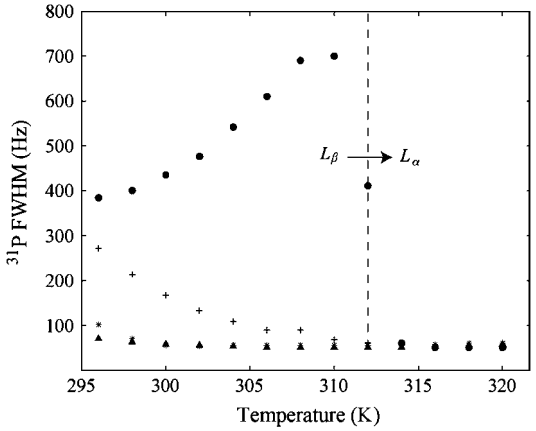

FIGURE 5 ^{31}P MAS NMR FWHM for SM resonance as a function of temperature in lipid bilayer mixtures: (•) SM, (*) DOPC/SM, (+) SM/Chol, and (▲) DOPC/SM/Chol.

indication of a change in motional correlation time. This increased line broadening might also be attributed to heterogeneities in the SM sample, resulting in a distribution of chemical shifts commonly observed in NMR spectra of disordered and/or heterogeneous systems. Contributions of the chemical shift distribution to the line width were estimated by measuring the ^{31}P MAS T_2 relaxation time, which is found to correlate well with the line width observations (see below). Therefore, it appears that for pure SM there is a restriction in some motional process before the main L_α transition. Similar observations have been made in DPPC (69) and 1,2-dimyristoyl-*sn*-glycero-3-phosphocholine (DMPC) (33), where the formation of a rippled phase, $P_{\beta'}$, occurs before the main transition. It has been shown by ^{14}N MAS NMR (70) and ^{31}P NMR (33) that some of the motional dynamics, particularly in the headgroup region, are slower in the $P_{\beta'}$ rippled phase than in the $L_{\beta'}$ gel phase or L_α liquid crystalline phase. This difference in dynamics has been detected as a broadening of the line width in the ^{14}N MAS NMR of DPPC and a decrease in ^{31}P T_2 relaxation time of DMPC in the $P_{\beta'}$ phase. This $P_{\beta'}$ rippled phase is usually detected as a distinct pretransition that occurs before the main L_α phase transition of saturated chain phosphatidylcholines like DPPC and DMPC using DSC. This distinct pretransition is not observed in the DSC of SM (68,69); however, some reports do indicate the existence of a rippled morphology in naturally occurring SM (69,71). The ^{31}P MAS NMR line width results presented here for pure SM further support the existence of a dynamically restricted, presumably $P_{\beta'}$ rippled phase in egg SM.

The ^{31}P FWHM of SM or DOPC in the other lipid mixtures (DOPC, DOPC/Chol, DOPC/SM, SM/Chol) do not show any indication of a similar dynamically restricted environment across the temperature range studied. The SM ^{31}P line width does decrease as the L_α phase transition is approached in the other mixtures, but it is not nearly as sharp as the transition observed for pure SM. These observations are consistent with reports on phosphatidylcholine/Chol mixtures that indicate a disappearance of the rippled phase pretransition in the presence of cholesterol for concentrations greater than 20% (72–75).

Variation of ^{31}P MAS NMR T_2 with temperature

To confirm that the trends observed in the ^{31}P FWHM were due to mobility variations and not chemical shift heterogeneities, the ^{31}P NMR T_2 relaxation times were measured across the same temperature range. The ^{31}P T_2 of pure SM and SM/Chol is shown in Fig. 6 *A* as a function of temperature. For the pure SM sample, the results are very similar to the ^{31}P FWHM results depicted in Fig. 4. The T_2 shows a decrease before the liquid crystalline phase transition that correlates well with the observed increase in the FWHM, followed by a large increase as the L_α phase transition is reached, and finally a leveling off as the transition is surpassed. The ^{31}P T_2 value for pure SM below L_α predicts a line width ~4 times narrower than the observed value. Therefore, it appears that below L_α, some of the SM ^{31}P line width contributions can be attributed to chemical shift distributions as a result of the heterogeneous nature of egg SM, and is in agreement with the multicomponent static ^{31}P powder pattern observed in Fig. 1 *A* (296 K). The decrease in ^{31}P T_2 observed before the L_α transition correlates well with the increase in the ^{31}P FWHM, arguing that this observed variation is the result of a decrease in headgroup dynamics. The decrease in the ^{31}P T_2 is again consistent with formation of a motionally restricted phase (similar to the rippled phase) before the L_α transition. In the SM/Chol mixture, the ^{31}P T_2 gradually increases until the L_α phase transition is reached, displaying no sign of this motionally restricted headgroup dynamic. Again, this is consistent with the previously observed elimination of the pretransition and rippled phase in DPPC mixtures with similar amounts of cholesterol (72–75). The phase transition of the SM/Chol mixture is significantly broader than the pure SM sample consistent with DSC results (76).

The ^{31}P T_2 as a function of temperature for SM in the DOPC/SM and DOPC/SM/Chol mixtures are displayed in Fig. 6 *B*. For DOPC/SM, the SM T_2 increases with a step at 306 K and the main L_α phase transition (314 K). The initial ^{31}P T_2 value is comparable to that observed in pure SM in the gel state, which suggests that SM in the DOPC/SM mixture is in a solid-ordered gel state below T_m. The slight dip in T_2 at 306 K could provide some evidence that there is a small gel-gel transition that is still observed similar to pure SM. In the raft-forming DOPC/SM/Chol lipid mixture, the ^{31}P T_2 of SM gradually increases toward the L_α phase transition and then levels off above 314 K. These trends are consistent with SM in the DOPC/SM/Chol mixture, being in a l_o state below T_m (T_2 between 9 and 10 ms), where the dynamics are not as slow as in the solid-ordered gel state that is observed for SM

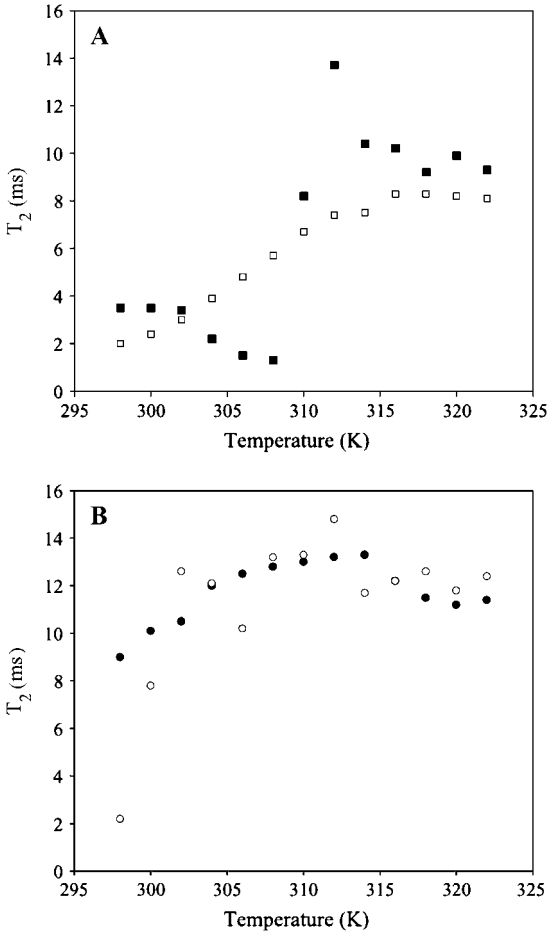

FIGURE 6 ^{31}P MAS NMR T_2 relaxation times measured for SM resonance with rotor synchronized spin-echo on MAS spectra as a function of temperature in lipid mixtures: (*A*) (■) SM and (□) SM/Chol, and (*B*) (○) DOPC/SM and (•) DOPC/SM/Chol.

in DOPC/SM ($T_2 = \sim 2$ ms) and still undergoes a broad phase transition to a l_d liquid crystalline state (T_2 between 11 and 13 ms). This transition is extremely broad, but observable by monitoring subtle variations in dynamics from T_2 measurements and the line width. The ^{31}P T_2 of DOPC remains relatively consistent across the temperature range in all the lipid mixtures studied with a value between 14.5 and 16.5 ms.

It is interesting to note the contributions from heteronuclear dipolar coupling to the ^{31}P line broadening observed for SM in these lipid mixtures. The ^{31}P MAS NMR spectra presented in this report were collected without ^{1}H decoupling. For pure SM (below T_m), the inclusion of ^{1}H decoupling narrows the line width from ~400 to ~200 Hz, demonstrating that residual ^{1}H-^{31}P dipolar coupling is still present under MAS at 2 kHz. Above T_m, there is no change in the ^{31}P MAS line widths with the incorporation of ^{1}H decoupling, demonstrating that in the L_α phase, any residual ^{1}H-^{31}P dipolar coupling is completely averaged by the combination of phospholipid headgroup motion and MAS. By obtaining ^{31}P MAS spectra without ^{1}H decoupling, subtle differences in headgroup dynamics could be distinguished by changes in the ^{31}P line width and T_2 due to the presence of the residual heteronuclear dipolar coupling. These small variations in headgroup dynamics were not readily determined from ^{31}P CSA variations.

Limits on time and length scales

The observation of powder patterns and spinning sidebands in the ^{31}P NMR spectra provides a way to determine limits for motional timescales and domain sizes. The CSA is the dominant nuclear interaction for ^{31}P, and scales linearly with magnetic field strength. For a 14.1 T magnetic field, the observed residual ^{31}P anisotropy of $\Delta\sigma \sim 42$ ppm, corresponds to a ~10 kHz interaction. As noted above, the lack of an observable isotropic resonance in the static spectra of any of the lipid mixtures investigated in this study demonstrates that there are no large-scale motions on a timescale <100 μs. In some systems, such rapid motions may exist for high curvature regions or isotropic phases, giving rise to a motionally averaged isotropic resonance; but that is not observed for the current DOPC/SM/Chol systems. The observation of typical, nondistorted ^{31}P CSA powder patterns and spinning sidebands patterns also provides a limit on the size of the MLV. It has been previously demonstrated that rapid lateral diffusion of the lipid along the curvature of the liposome results in a change of the lipid normal orientation with respect to the magnetic field and can give rise to averaging or exchange of different frequencies within the ^{31}P CSA pattern. This liposome radius (R) is related to the effective lipid lateral diffusion (τ_D) by $R = \sqrt{6D_L\tau_D}$, where D_L is the lateral diffusion coefficient. Recent PFG ^{1}H NMR measurements of D_L in the DOPC/SM/CHOL raft-forming mixture have measured D_L to range between 1 and 10 $\times$ 10^{-12} m^2/s, depending on the temperature, cholesterol content, phase (l_o versus l_d), and the lipid measured (77). For this range of diffusion constants, the lack of a distorted CSA line shape limits the curvature to $R \gg 50$ nm. This is consistent with ^{31}P two-dimensional exchange experiments that have measured the radii in pure lipid MLV between 300 and 1000 nm (78,79).

For the DOPC/SM and the raft-forming DOPC/SM/Chol mixture below T_m, the lack of discernable different CSA patterns overlapping for SM (or DOPC) would suggest that SM is predominantly incorporated in the l_o phase, with no or a very low concentration in the l_d (L_α) phase that is predominantly DOPC (see additional discussion above in section on variation of ^{31}P CSA for mixtures). The other possibility is that the ^{31}P CSA observed is a weighted average due to rapid exchange of the lipids between the l_o and l_d phase on the timescale of hundreds of microseconds (assuming a ~10 ppm difference in the CSA between l_o and l_d phases). This averaging would require very small domain

sizes on the order of tens of nanometers. Interestingly, recent PFG NMR studies on this ternary lipid mixture found that the exchange between the phases was slow on the PFG timescale of 50–250 ms. Obviously, additional studies will be required to unravel this information.

The final timescale limit involves the variation of line width in SM as a function of temperature (Fig. 5). Based on the differences between the line width with and without ^{1}H decoupling, there is a residual heteronuclear ^{1}H-^{31}P dipolar coupling under MAS of ~200 Hz. The sensitivity of the line width during this temperature range suggests that motions on the 5 ms timescale are occurring in SM during the phase transition. This timescale is slower, but consistent, with an increased rotational correlation time (~30 μs) of SM compared to DMPC reported by Malcolm and co-workers (34). These longer SM correlation times were attributed to the existence of inter- and intramolecular hydrogen bonding in SM.

CONCLUSIONS

The ^{31}P MAS NMR for the model lipid membrane mixtures SM, SM/Chol, DOPC, DOPC/Chol, SM/DOPC, and SM/DOPC/Chol have been obtained. The ^{31}P MAS NMR is complementary to static ^{31}P NMR measurements and allowed the ability to resolve the SM and DOPC lipids within raft-forming mixtures. The individual ^{31}P CSA parameters were measured for the SM and DOPC components that comprise the l_o and l_d phases within these mixtures. The ^{31}P MAS line widths and T_2 measurements detected subtle differences in the headgroup dynamics for the different lipids as a function of mixture composition and temperature. These ^{31}P MAS NMR results show that cholesterol is not completely excluded from the DOPC l_d domains during raft formation. Similarly, the headgroup dynamics support a l_o state for SM below T_m in the ternary mixture. These results also highlight cooperative lipid effects within these raft-forming mixtures and demonstrate that ^{31}P MAS NMR is a powerful tool for probing raft formation in the more complex ternary samples.

These ^{31}P NMR results provide additional insight into the current view of raft formation in lipid systems. Two main arguments are typically presented when discussing the formation of raft phases from a molecular point of view. The first argument is that chain-packing effects (i.e., cholesterol prefers to interact with saturated chain lipids over unsaturated lipids) help drive lipid raft formation. Headgroup interactions may also play an indirect role in chain packing. The second molecular interaction forwarded for impacting raft formation is the potential for hydrogen-bond formation between the cholesterol OH moiety and the lipid backbone and/or hydrogen bonding between lipid headgroups. In the case of SM, the cholesterol/lipid interaction can occur at the OH, NH, or carbonyl sites, and may involve bridging water molecules between the sphingolipid and OH of cholesterol. Currently, the chain-packing argument appears to be favored when discussing the main driving force for phase separation into coexisting liquid phases. These chain-packing effects are most directly measured using ^{2}H NMR, and as such will be the molecular level interactions highlighted by such studies. However, headgroup and backbone interactions need to be explicitly considered, especially in light of the impact of DOPC on the SM headgroup dynamics shown in this study along with recent results that indicate cholesterol prefers SM over DPPC in model raft formers (22). SM and DPPC have identical headgroups, similar saturated chain lengths, and a comparable T_m, but have substantially different backbones. These observations suggest that the sphingosine backbone may influence the preference of cholesterol for sphingolipids over glycerophospholipids. The ^{31}P MAS NMR results presented here show that there are subtle variations in the headgroup dynamics of SM in raft-forming mixtures and may provide some evidence for variability in inter- and intramolecular hydrogen bonding motifs when cholesterol-rich SM rafts are formed. It is clear that any future models describing the formation of rafts in lipid mixtures must include the impact on both acyl chain and headgroup dynamics, and that ^{31}P MAS NMR provides an alternative probe of these dynamics.

This work was supported by the Sandia Laboratory Directed Research Development program. Sandia is a multiprogram laboratory operated by Sandia Corporation, a Lockheed Martin company, for the United States Department of Energy's National Nuclear Security Administration under contract DE-AC04-94AL85000.

REFERENCES

1. Simons, K., and E. Ikonen. 1997. Functional rafts in cell membranes. *Nature*. 387:569–572.
2. Anderson, R. G. W., and K. Jacobson. 2002. A role for lipid shells in targeting proteins to caveolae, rafts, and other lipid domains. *Science*. 296:1821–1825.
3. Binder, W. H., V. Barragan, and F. M. Menger. 2003. Domains and rafts in lipid membranes. *Angew. Chem. Int. Ed. Engl.* 42:5802–5827.
4. Simons, K., and D. Toomre. 2000. Lipid rafts and signal transduction. *Nat. Rev. Mol. Cell Biol.* 1:31–39.
5. Ikonen, E. 2001. Roles of lipid rafts in membrane transport. *Curr. Opin. Cell Biol.* 13:470–477.
6. Brown, D. A., and E. London. 1998. Function of lipid rafts in biological membranes. *Annu. Rev. Cell Dev. Biol.* 14:111–136.
7. Baron, G. S., K. Wehrly, D. W. Dorward, B. Chesebro, and B. Caughey. 2002. Conversion of raft associated prion protein to the protease-resistant state requires insertion of PrP-res (PrP^{Sc}) into contiguous membranes. *EMBO J.* 21:1031–1040.
8. Kakio, A., S. Nishimoto, K. Yanagisawa, Y. Kozutsumi, and K. Matsuzaki. 2002. Interactions of amyloid β-protein with various gangliosides in raft-like membranes: importance of GM1 ganglioside-bound form as an endogenous seed for Alzheimer amyloid. *Biochemistry*. 41:7385–7390.
9. van der Goot, F. G., and T. Harder. 2001. Raft membrane domains: from a liquid-ordered membrane phase to a site of pathogen attack. *Semin. Immunol.* 13:89–97.
10. Puri, A., P. Hug, K. Jernigan, J. Barchi, H.-J. Kim, J. Hamilton, J. Wiels, G. J. Murray, R. O. Brady, and R. Blumenthal. 1998. The

neutral glycosphingolipid globotriaosylceramide promotes fusion mediated by a CD4-dependent CXCR4-utilizing HIV type 1 envelope glycoprotein. *Proc. Natl. Acad. Sci. USA.* 95:14435–14440.

11. Mañes, S., G. del Real, R. A. Lacalle, P. Lucas, and C. Gómez-Moutón. 2000. Membrane raft microdomains mediate lateral assemblies required for HIV-1 infection. *EMBO Rep.* 1:190–196.
12. Liao, Z., L. M. Cimakasky, R. Hampton, D. H. Nguyen, and J. E. K. Hildreth. 2001. Lipid rafts and HIV pathogenesis: host membrane cholesterol is required for infection by HIV type 1. *AIDS Res. Hum. Retroviruses.* 17:1009–1019.
13. Brown, D. A., and E. London. 1997. Structure of detergent-resistant membrane domains: does phase separation occur in biological membranes? *Biochem. Biophys. Res. Commun.* 240:1–7.
14. Veatch, S. L., and S. L. Keller. 2005. Miscibility phase diagrams of giant vesicles containing sphingomyelin. *Phys. Rev. Lett.* 94:148101.
15. Baumgart, T., S. T. Hess, and W. W. Webb. 2003. Imaging coexisting fluid domains in biomembrane models coupling curvature and line tension. *Nature.* 425:821–824.
16. Veatch, S. L., I. V. Polozov, K. Gawrisch, and S. L. Keller. 2002. Organization in lipid membranes containing cholesterol. *Phys. Rev. Lett.* 89:268101.
17. Veatch, S. L., I. V. Polozov, K. Gawrisch, and S. L. Keller. 2004. Liquid domains in vesicles investigated by NMR and fluorescence microscopy. *Biophys. J.* 86:2910–2922.
18. Veatch, S. L., and S. L. Keller. 2003. Separation of liquid phases in giant vesicles of ternary mixtures of phospholipids and cholesterol. *Biophys. J.* 85:3074–3083.
19. Dietrich, C., L. A. Bagatolli, Z. N. Volovyk, N. L. Thompson, M. Levi, K. Jacobson, and E. Gratton. 2001. Lipid rafts reconstituted in model membranes. *Biophys. J.* 80:1417–1428.
20. Filippov, A., G. Orädd, and L. Göran. 2004. Lipid lateral diffusion in ordered and disordered phases in raft mixtures. *Biophys. J.* 86:891–896.
21. Collado, M. I., F. M. Goñi, A. Alonso, and D. Marsh. 2005. Domain formation in sphingomyelin/cholesterol mixed membranes studied by spin-label electron spin resonance spectroscopy. *Biochemistry.* 44: 4911–4918.
22. van Duyl, B. Y., D. Ganchev, V. Chupin, B. de Kruijff, and J. A. Killian. 2003. Sphingomyelin is much more effective than saturated phosphatidylcholine in excluding unsaturated phosphatidylcholine from domains formed with cholesterol. *FEBS Lett.* 547:101–106.
23. Rinia, H. A., M. M. E. Snel, J. P. J. M. van der Eerden, and B. de Kruijff. 2001. Visualizing detergent resistant domains in model membranes with atomic force microscopy. *FEBS Lett.* 501:92–96.
24. Chachaty, C., D. Rainteau, C. Tessier, P. J. Quinn, and C. Wolf. 2005. Building up of the liquid-ordered phase formed by sphingomyelin and cholesterol. *Biophys. J.* 88:4032–4044.
25. Nicolini, C., P. Thiyagarajan, and R. Winter. 2004. Small-scale composition fluctuations and microdomain formation in lipid raft models as revealed by small-angle neutron scattering. *Phys. Chem. Chem. Phys.* 6:5531–5534.
26. de Almeida, R. F. M., A. Fedorov, and M. Prieto. 2003. Sphingomyelin/phosphatidylcholine/cholesterol phase diagram: boundaries and composition of lipid rafts. *Biophys. J.* 85:2406–2416.
27. Radhakrishnan, A., and H. McConnell. 2005. Condensed complexes in vesicles containing cholesterol and phospholipids. *Proc. Natl. Acad. Sci. USA.* 102:12662–12666.
28. Seelig, J., and H.-U. Gally. 1976. Investigation of phosphatidylethanolamine bilayers by deuterium and phosphorous-31 nuclear magnetic resonance. *Biochemistry.* 15:5199–5204.
29. Seelig, J. 1978. ^{31}P nuclear magnetic resonance and the head group structure of phospholipids in membranes. *Biochim. Biophys. Acta.* 515:105–140.
30. Niederberger, W., and J. Seelig. 1976. Phosphorous-31 chemical shift anisotropy in unsonicated phospholipid bilayers. *J. Am. Chem. Soc.* 98:3704–3706.
31. Griffin, R. G., L. Powers, and P. S. Pershan. 1978. Head-group conformation in phospholipids: A phosphorous-31 nuclear magnetic resonance study of oriented monodomain dipalmitoylphosphatidylcholine bilayers. *Biochemistry.* 17:2718–2722.
32. Campbell, R. F., E. Melrovitch, and J. H. Freed. 1979. Slow-motional NMR line shapes for very anisotropic rotational diffusion. Phosphorous-31 NMR in phospholipids. *J. Phys. Chem.* 83:525–533.
33. Dufourc, E. J., C. Mayer, J. Stohrer, G. Althoff, and G. Kothe. 1992. Dynamics of phosphate headgroups in biomembranes comprehensive analysis using phosphorous-31 nuclear magnetic resonance lineshape and relaxation time measurements. *Biophys. J.* 61:42–57.
34. Malcolm, I. C., J. C. Ross, and J. Higinbotham. 2005. A study of the headgroup motion of sphingomyelin using ^{31}P NMR and an analytically soluble model. *Solid State Nucl. Magn. Reson.* 27:247–256.
35. Brown, M. F., and J. Seelig. 1978. Influence of cholesterol on the polar region of phosphatidylcholine and phosphatidylethanolamine bilayers. *Biochemistry.* 17:381–384.
36. Cullis, P. R., and M. J. Hope. 1980. The bilayer stabilizing role of sphingomyelin in the presence of cholesterol: a ^{31}P NMR study. *Biochim. Biophys. Acta.* 597:533–542.
37. Griffin, R. G. 1976. Observation of the effect of water on the ^{31}P nuclear magnetic resonance spectra of dipalmitoyllecithin. *J. Am. Chem. Soc.* 98:851–853.
38. Shaikh, S. R., M. R. Brzustowicz, N. Gustafson, W. Stillwell, and S. R. Wassall. 2002. Monounsaturated PE does not phase-separate from the lipid raft molecules sphingomyelin and cholesterol: role for polyunsaturation? *Biochemistry.* 41:10593–10602.
39. Hao, Y.-H., and J.-W. Chen. 2001. Influence of cholesterol on the biophysical properties of the sphingomyelin/DOPC binary system. *J. Membr. Biol.* 183:85–92.
40. Heerklotz, H. 2002. Triton promotes domain formation in lipid raft mixtures. *Biophys. J.* 83:2693–2701.
41. Aussenac, F., M. Tavares, and E. J. Dufourc. 2003. Cholesterol dynamics in membranes of raft composition: a molecular point of view from ^{2}H and ^{31}P solid-state NMR. *Biochemistry.* 42:1383–1390.
42. Guo, W., and J. A. Hamilton. 1995. A multinuclear solid-state NMR study of phospholipid-cholesterol interactions. Dipalmitoylphosphatidylcholine-cholesterol binary system. *Biochemistry.* 34:14174–14184.
43. Spooner, P. J. R., and A. Watts. 1992. Cytochrome *c* interactions with cardiolipin in bilayers: a multinuclear magic-angle spinning NMR study. *Biochemistry.* 31:10129–10138.
44. Pinheiro, T. J. T., and A. Watts. 1994. Resolution of individual lipids in mixed phospholipid membranes and specific lipid-cytochrome c interactions by magic-angle spinning solid-state phosphorous-31 NMR. *Biochemistry.* 33:2459–2467.
45. Warschawski, D. E., P. Fellmann, and P. F. Devaux. 1996. High-resolution ^{31}P-^{1}H two-dimensional nuclear magnetic resonance spectra of unsonicated lipid mixtures spinning at the magic-angle. *Eur. Biophys. J.* 25:131–137.
46. Bonev, B. B., W. C. Chan, B. W. Bycroft, G. C. K. Roberts, and A. Watts. 2000. Interaction of the lantibiotic nisin with mixed lipid bilayers: A ^{31}P and ^{2}H NMR study. *Biochemistry.* 39:11425–11433.
47. Bonev, B., A. Watts, M. Bokvist, and G. Gröbner. 2001. Electrostatic peptide-lipid interactions of amyloid-β peptide pentalysine with membrane surfaces monitored by ^{31}P MAS NMR. *Phys. Chem. Chem. Phys.* 3:2904–2910.
48. Bokvist, M., F. Lindström, A. Watts, and G. Gröbner. 2004. Two types of Alzheimer's β-amyloid (1–40) peptide membrane interactions: aggregation preventing transmembrane anchoring versus accelerated surface fibril formation. *J. Mol. Biol.* 335:1039–1049.
49. Lindström, F., P. T. F. Williamson, and G. Gröbner. 2005. Molecular insight into the electrostatic membrane surface potential by ^{14}N/^{31}P MAS NMR spectroscopy: nociceptin-lipid association. *J. Am. Chem. Soc.* 127:6610–6616.
50. Traïkia, M., D. E. Warschawski, M. Recouvreur, J. Cartaud, and P. F. Devaux. 2000. Formation of unilamellar vesicles by repetitive

freeze-thaw cycles: characterization by electron microscopy and ^{31}P-nuclear magnetic resonance. *Eur. Biophys. J.* 29:184–195.

51. Bennett, A. E., C. M. Rienstra, M. Auger, K. V. Lakshmi, and R. G. Griffin. 1995. Heteronuclear decoupling in rotating solids. *J. Chem. Phys.* 103:6951–6958.
52. Massiot, D., F. Fayon, M. Capron, I. King, S. LeCalvé, B. Alonso, J.-O. Durand, B. Bujoli, Z. Gan, and G. Hoatson. 2002. Modelling one- and two-dimensional solid-state NMR spectra. *Magn. Reson. Chem.* 40:70–76.
53. Tenchov, B. 1991. On the reversibility of the phase transitions in lipid water systems. *Chem. Phys. Lipids.* 57:165–177.
54. Calhoun, W. I., and G. G. Shipley. 1979. Sphingomyelin-lecithin bilayers and their interaction with cholesterol. *Biochemistry.* 18:1717–1722.
55. Ruiz-Argüello, M. B., M. P. Veiga, J. L. R. Arrondo, F. M. Goñi, and A. Alonso. 2002. Sphingomyelinase cleavage of sphingomyelin in pure and mixed lipid membranes. Influence of the physical state of the sphingolipid. *Chem. Phys. Lipids.* 114:11–20.
56. Bruzik, K. S., B. Sobon, and G. M. Salamonczyk. 1990. Nuclear magnetic resonance study of sphingomyelin bilayers. *Biochemistry.* 29:4017–4021.
57. Smith, I. C. P., and I. H. Ekiel. 1984. Phosphorous-31 NMR of Phospholipids in Membranes. Phosphorous-31 NMR: Principles and Applications. D. Gorenstein, editor. Academic Press, London.
58. Cullis, P. R., B. de Kruijff, and R. E. Richards. 1976. Factors affecting the motion of the polar headgroup in phospholipid bilayers: a 31P NMR study of unsonicated phosphatidylcholine liposomes. *Biochim. Biophys. Acta.* 426:433–446.
59. Davis, J. H. 1983. The description of membrane lipid conformation, order and dynamics by ^{2}H-NMR. *Biochim. Biophys. Acta.* 737:117–171.
60. Dubinnyi, M. A., D. M. Lesovoy, P. V. Dubovskii, V. V. Chupin, and A. S. Arseniev. 2006. Modeling of ^{31}P-NMR spectra of magnetically oriented phospholipid liposomes: a new analytical solution. *Solid State Nucl. Magn. Reson.* 29:305–311.
61. Schäfer, H., B. Mädler, and E. Sternin. 1998. Determination of orientational order parameters from ^{2}H NMR spectra of magnetically partially oriented lipid bilayers. *Biophys. J.* 74:1007–1014.
62. Hodgkinson, P., and L. Emsley. 1997. The reliability of the determination of tensor parameters by solid-state nuclear magnetic resonance. *J. Chem. Phys.* 107:4808–4816.
63. Chiu, S. W., S. Vasudevan, E. Jakobsson, R. J. Mashl, and H. L. Scott. 2003. Structure of sphingomyelin bilayers: a simulation study. *Biophys. J.* 85:3624–3635.
64. Niemelä, P., M. T. Hyvönen, and I. Vattulainen. 2004. Structure and dynamics of sphingomyelin bilayer: insight gained through systematic comparison to phosphatidylcholine. *Biophys. J.* 87:2976–2989.
65. Talbott, C. M., I. Vorobyov, D. Borchman, K. G. Taylor, D. B. DuPré, and M. C. Yappert. 2000. Conformational studies of sphingolipids by NMR spectroscopy. II. Sphingomyelin. *Biochim. Biophys. Acta.* 1467:326–337.
66. Schmidt, C. F., Y. Barenholz, and T. E. Thompson. 1977. A nuclear magnetic resonance study of sphingomyelin in bilayer systems. *Biochemistry.* 16:2649–2656.
67. Bruzik, K. S., and M.-D. Tsai. 1987. A calorimetric study of the thermotropic behavior of pure spingomyelin diastereomers. *Biochemistry.* 26:5364–5368.
68. Barenholz, Y., J. Suurkuusk, D. Mountcastle, T. E. Thompson, and R. L. Biltonen. 1976. A calorimetric study of the thermotropic phase behavior of aqueous dispersions of natural and synthetic sphingomyelins. *Biochemistry.* 15:2441–2447.
69. Meyer, H. W., H. Bunjes, and A. S. Ulrich. 1999. Morphological transitions of brain sphingomyelin are determined by the hydration protocol: ripples re-arrange in plane, and sponge-like networks disintegrate into small vesicles. *Chem. Phys. Lipids.* 99:111–123.
70. Sparrman, T., and P.-O. Westlund. 2003. An NMR line shape and relaxation analysis of heavy water powder spectra of the L_{α}, $L_{\beta'}$, and $P_{\beta'}$ phases in the DPPC/water system. *Phys. Chem. Chem. Phys.* 5: 2114–2121.
71. Hui, S. W., T. P. Stewart, and P. L. Yeagle. 1980. Temperature dependent morphological and phase behavior of sphingomyelin. *Biochim. Biophys. Acta.* 601:271–281.
72. Koynova, R. D., A. I. Boyanov, and B. G. Tenchov. 1985. On the phase diagram of an L-dipalmitoylphosphatidycholine/cholesterol mixture. *FEBS Lett.* 187:65–68.
73. Mortensen, K., W. Pfeiffer, E. Sackmann, and W. Knoll. 1988. Structural properties of a phosphatidylcholine-cholesterol system as studied by small-angle neutron scattering: ripple structure and phase diagram. *Biochim. Biophys. Acta.* 945:221–245.
74. Meyer, H. W., K. Semmier, and P. J. Quinn. 1997. The effect of sterols on structures formed in the gel/subgel phase state of dipalmitoylphosphatidycholine bilayers. *Mol. Membr. Biol.* 14:187–193.
75. Meyer, H. W., W. Richter, and G. Brezesinski. 1994. Convex-concave curvatures in bilayers of dipalmitoylphophatidylcholine and cholesterol induced by amphotericin B/deoxycholate after prolonged storage. *Biochim. Biophys. Acta.* 1190:9–19.
76. Maulik, P. R., and G. G. Shipley. 1996. *N*-palmitoyl sphingomyelin bilayers: structure and interactions with cholesterol and dipamitoylphosphatidylcholine. *Biochemistry.* 35:8025–8034.
77. Orädd, G., and G. Lindblom. 2004. Lateral diffusion studied by pulse field gradient NMR on oriented lipid membranes. *Magn. Reson. Chem.* 42:123–131.
78. Fenske, D. B., and H. C. Jarrell. 1991. Phosphorous-31 two-dimensional solid-state exchange NMR. *Biophys. J.* 59:55–69.
79. Picard, F., M.-J. Paquet, E. K. DuFourc, and M. Auger. 1998. Measurement of the lateral diffusion of dipalmitoylphophatidylcholine adsorbed on silica beads in the absence and presence of melittin: A ^{31}P two-dimensional exchange solid state NMR study. *Biophys. J.* 74:857–868.